Experimental and numerical studies of pin-ended press-braked S960 ultra-high strength steel channel section columns

Fangying Wang[a], Yating Liang[b], Ou Zhao[*a]

[a] School of Civil and Environmental Engineering, Nanyang Technological University, Singapore

[b] School of Engineering, University of Glasgow, Glasgow, UK

[*] Corresponding author, Email: ou.zhao@ntu.edu.sg

Abstract

Grade S960 ultra-high strength steel is receiving increasing attention owing to its excellent strength-to-weight ratio. However, its application in construction engineering is rather limited due to the lack of adequate design rules, as the current established codes in Europe, North America and Australia/New Zealand only cover the design of steel components with material grades up to S700 (or S690). This prompts investigations into different types of S960 UHSS structural components and development of precise and efficient design rules for them. The present paper focuses on press-braked S960 UHSS channel section columns prone to flexural buckling about the minor principal axes, with their behaviour and strengths thoroughly examined through experiments and numerical modelling. An experimental programme was firstly performed on two non-slender press-braked channel sections, with five column specimens of varying member lengths employed for each cross-section, and included initial local and global geometric imperfection measurements and pin-ended column tests about the minor principal axes. This was followed by a parallel numerical modelling programme, in which finite element (FE) models were developed to simulate the experimental results and afterwards adopted to perform parametric studies to derive additional numerical data over a broader spectrum of cross-section dimensions and member lengths. It is worth noting that there were two orientations associated with minor-axis flexural buckling of press-braked S960 UHSS channel section columns, namely ‘C’ orientation (indicating that columns buckled towards the webs) and ‘reverse C’ orientation (indicating that columns buckled towards the flange tips), and both of the two types of failure modes were carefully examined in the present study. It was found that channel section columns failing by flexural buckling in the ‘reverse C’ orientation generally exhibited superior strengths relative to their counterparts with failure in the ‘C’ orientation. The experimental and numerical data were also used to assess the applicability of the codified provisions for press-braked S700 (or S690) channel section columns failing by minor-axis flexural buckling to the design of their S960 counterparts. The assessment results indicated that (i) the existing European code leads to overall conservative and scattered design flexural buckling strengths, especially for those relatively short and intermediate press-braked S960 UHSS channel section columns with failure in the ‘reverse C’ orientation, and (ii) the North American specification and Australian/New Zealand standard result in a higher degree of design accuracy and consistency than the European code, but with many over-predicted flexural buckling strengths for press-braked S960 UHSS channel section short and intermediate columns failing in the ‘C’ orientation.

Keywords: ‘C’ orientation; Design codes; Flexural buckling behaviour; Grade S960 ultra-high strength steel; Minor principal axis; Numerical modelling; Pin-ended column tests; Press-braked channel section; ‘Reverse C’ orientation

1. Introduction

High strength steels (HSS), defined as steels with yield strengths greater than 460 MPa, are becoming increasingly widespread in civil engineering, owing to their superior strength-to-weight ratios compared to the conventional normal strength steels. The use of high strength steel allows structural components to be designed with smaller dimensions, thereby achieving reductions in overall structure and foundation weights. This makes high strength steels a desirable material and particularly well suited to high-rise and long-span structures [1,2]. It is worth noting that S690 (or S700) is the highest material grade covered in the existing international design standards. However, recent advancements in material science and manufacturing techniques have enabled production of high strength steels with yield strengths greater than 700 MPa (even up to 1200 MPa) but still good weldability and ductility [3,4]. Grade S960 ultra-high strength steel (UHSS), with the nominal yield strength equal to 960 MPa, is a typical example and currently mainly used in the automotive industry. In order to extend the application of Grade S960 ultra-high strength steel to construction industry, research efforts have been made towards verifying the behaviour of various types of S960 UHSS cross-sections and members and devising accurate design provisions for them. Specifically, Li et al. [1] conducted stub column tests on S960 UHSS welded I- and box sections to investigate their local buckling behaviour and cross-section compression resistances; it was found that the codified slenderness limits for S690 (or S700) HSS plate elements are generally applicable to their S960 UHSS counterparts, though more accurate slenderness limits were also proposed based on the test results. Similar investigations into the local stability and compression resistances of S960 UHSS welded I- and box section stub columns were performed by Shi et al. [5]; comparisons of the test and numerical failure loads against the predicted failure loads indicated a high level of inaccuracy of the codified design rules when applied to S960 UHSS welded I- and box section stub columns. Ma et al. [6,7] conducted tests on S960 UHSS cold-formed tubular section stub columns and beams, and highlighted the inapplicability of the relevant codified local buckling design provisions when used for S960 UHSS cold-formed tubular section components. Shi et al. [8] and Ban et al. [9] experimentally and numerically examined the flexural buckling behaviour and strengths of S960 UHSS welded I- and box section columns, highlighted the inaccuracy of the codified design buckling curves, and finally proposed new improved design methods.

Despite extensive studies have been carried out on S960 UHSS doubly symmetric sections (i.e. welded I- and box sections and cold-formed tubular sections), investigations into their non-doubly symmetric counterparts are rather limited. Therefore, an in-depth research programme has been initiated by the authors, with the aim of investigating the static, fire and post-fire performance of various types of S960 UHSS angle and channel section structural components. Investigations into the cross-section compressive behaviour of S960 UHSS angle and channel section stub columns [10] and flexural responses of S960 UHSS channel section beams [11] have been recently performed, whilst the flexural buckling behaviour of S960 UHSS channel section columns is thoroughly examined based on experiments and numerical modelling, and fully presented in this paper.

First, a structural testing programme was carried out on two press-braked S960 UHSS channel sections, with five column specimens of varying member lengths adopted for each cross-section, and included initial local and global geometric imperfection measurements and pin-ended column tests about the minor principal axes. A complementary numerical modelling programme was then carried out, and included a validation study to validate the developed column finite element models against the experimental results and a parametric study to derive further numerical data over a broader spectrum of cross-section dimensions and member lengths. The experimental and numerical data were analysed and employed to assess the applicability of the relevant codified provisions for press-braked S700 (or S690) HSS channel section columns prone to minor-axis flexural buckling, prescribed in EN 1993-1-3 [12], AISI S100 [13] and AS/NZS 4600 [14], to the design of their S960 UHSS counterparts.

2. Laboratory testing

2.1. Overview

A comprehensive laboratory testing programme was firstly conducted to experimentally examine the minor-axis flexural buckling behaviour and strengths of pin-ended press-braked S960 UHSS channel section columns. Two different channel sections were taken into account in the laboratory testing programme: C 70×40×6 and C 80×45×6, both of which are classified as Class 1 according to the slenderness limits prescribed in EN 1993-1-1 [15] and EN 1993-1-12 [16], and also fall in the category of non-slender sections specified in AISI S100 [13] and AS/NZS 4600 [14]. Both of the adopted channel sections were press-braked from 6 mm thick S960 UHSS sheets. For each channel section size, five specimens with various member lengths were prepared. Each specimen was first cut to the pre-defined nominal length using a band saw, and then milled flat and square at both ends in a CNC milling machine. The cross-section dimensions, including the outer flange width B_f, the outer web width B_w, the wall thickness t and the inner corner radius r_i – see Fig. 1, and the member length L of each specimen were accurately measured prior to pin-ended column tests, and are reported in Table 1. The specimen label comprises the cross-section identifier 'C1' or 'C2' ('C1' representing C 70×40×6 and 'C2' standing for C 80×45×6), a letter 'L (indicating length) and a number (for the purpose of differentiating specimens with the same cross-section size but different member lengths). In the following sections, material tensile coupon tests and results, previously reported in detail by the authors in Wang et al. [10], are firstly reviewed; this is followed by descriptions of initial global and local geometric imperfection measurements of the column specimens and pin-ended column tests.

2.2. Material tensile coupon tests

Prior to pin-ended column tests, tensile coupon tests were performed to obtain the material properties of the two adopted press-braked S960 UHSS channel sections; the material test setups and results have been fully described in Wang et al. [10], and are briefly reviewed herein. Given that both of the two adopted channel sections were press-braked from the same batch of S960 UHSS sheets using the same set of punch and die, their material properties were deemed to have very little if any difference. Coupons were therefore only machined from the web, flange and corner of a representative channel section C 70×40×6 – see Fig. 1, and one additional coupon was also extracted from the virgin sheet. The flat coupons cut from the flange and web of the channel section C 70×40×6 and virgin sheet are respectively denoted as C 70×40×6-F, C 70×40×6-W and VS, while the corner coupon cut from the corner portion of the channel section C 70×40×6 is labelled as C 70×40×6-C. The geometric sizes of both the flat and corner coupons complied with the requirements given in ASTM E8M-15 [17], and all the coupons were carefully machined such that the widths of the parallel necked portions, as measured by micrometer, were equal to 12 mm. The measured full stress–strain curves of the flat and corner coupons are shown in Fig. 2. A summary of the key material properties obtained from the tensile coupon tests is presented in Table 2, in which E is the Young's modulus, f_y and

f_u are the yield and ultimate stresses, respectively, ε_u is the strain at the ultimate stress, and ε_f is the strain at fracture.

2.3. Initial local and global geometric imperfection measurements

Initial geometric imperfections inherently exist in thin-walled steel members and are known to affect their structural behaviour and capacities [18–21]. The initial global and local geometric imperfections of each press-braked S960 UHSS channel section column specimen were therefore measured. The setup for initial global geometric imperfection measurements is depicted in Fig. 3(a), where a calibrated CNC router table is utilised to provide a flat work bench for mounting the specimen, and a LVDT, fixed onto the arm of the CNC router, is moved along the centreline of the specimen web to record the deviations in the direction of minor-axis flexural buckling. The initial global geometric imperfections of each specimen were defined as the deviations from a linear reference line (i.e. a straight line connecting the data points recorded by the LVDT at the two ends). Fig. 4(a) and Fig. 4(b) depict the initial global geometric imperfection distribution profiles measured for the C 70×40×6 and C 80×45×6 column specimens, respectively, while the measured initial global geometric imperfection amplitude of each column specimen at mid-height ω_g is reported in Table 1; note that the measured initial global geometric imperfection amplitudes are taken as positive if the imperfection profiles are towards the flange tips – see Fig. 5(a), but are negative if the imperfection profiles are towards the webs – see Fig. 5(b). The rig for initial local geometric imperfection measurements, as shown in Fig. 3(b), is similar to that used for initial global geometric imperfection measurements. But it is worth noting that the initial local geometric imperfections of each specimen were measured along the centrelines of the three constituent plate elements (two flanges and one web) over the central 300 mm; this length is deemed short enough to eliminate the influence from member initial global geometric imperfections, but still long enough to incorporate representative initial local geometric imperfections. For each constituent plate element of the specimen, the initial local geometric imperfections were taken as the derivations from a linear regression line fitted to the corresponding measured data set [10,11,22,23], while the initial local geometric imperfection magnitude of the specimen ω_0 was defined as the largest derivation derived from all the three constituent plate elements, as presented in Table 1. Note that the manufacturing squareness tolerance for flanges of structural channel sections is equal to 2 mm when $B_f \leqslant 100$ and the corresponding tolerances for channel webs are equal to 0.5 mm and 1.0 mm when $B_w \leqslant 100$ mm and $100 < B_w \leqslant 200$ mm, respectively. The measured initial geometric imperfections, as listed in Table 1, are smaller than the corresponding codified manufacturing tolerances. The measured initial local geometric imperfection distributions of the outstand flanges and internal web of a typical press-braked S960 UHSS channel section column specimen C2-L3 are plotted in Fig. 6.

2.4. Pin-ended column tests

Compression tests on ten pin-ended press-braked S960 UHSS channel section columns were performed to examine their minor-axis flexural buckling behaviour and capacities. All the column specimens were concentrically compressed in an INSTRON 5000 kN capacity servo-controlled hydraulic testing machine at a constant rate of 0.2 mm/min. The testing machine was equipped with knife-edge and anchor devices at both ends, which offer pin-ended boundary conditions to the column specimens, i.e. allowing for rotation about the buckling axis but restraining rotations about other axes as well as twisting and warping. As depicted in Fig. 7, the knife-edge device consists of a pit plate with a semi-circular groove and a wedge plate with a knife-edge wedge, while the anchor device consists of a 20 mm thick hardened base plate and four 15 mm thick stiffening plates. Prior to testing, the column specimen, together with the hardened base plates at both ends, was firstly positioned between the top and bottom wedge plates, with its cross-section minor principal axis parallel to the knife-edges and its member longitudinal axis intersecting with the knife-edges at right angles, and then anchored at both ends using the four stiffening plates (bolted to the wedge plates), before placed between the top and bottom pit plates in the testing machine. It is worth noting that the distance measured from the end of the specimen to the rotation centre of the knife-edge device is equal to 75 mm. Table 3 lists the effective member length of each column specimen L_e=L+150 mm and the corresponding member non-dimensional slenderness $\bar{\lambda}$ about the minor principle axis, as calculated from Eq. (1), where A is the gross cross-section area and I is the second moment of area about the minor principle axis.

$$\bar{\lambda} = \sqrt{\frac{Af_y L_e^2}{\pi^2 EI}} \quad (1)$$

The instrumentation employed for pin-ended column tests is shown in Fig. 7, where a LVDT is horizontally installed at the mid-height of the column specimen, to record the lateral deflection along the buckling direction, and two pairs of strain gauges are attached to the outstand flanges at mid-height and at the same time offset from the cross-section minor principal axis to each side by the same distance (see Fig. 7), to monitor the longitudinal strains at these locations. For each channel section column specimen, the readings from the LVDT and strain gauges were adopted to derive the overall loading eccentricity relative to the minor principal axis of the cross-section at mid-height e_m, based on Eq. (2) [24–28], where ε_{max}-ε_{min} is the difference of the longitudinal strains measured by the two pairs of strain gauges, N is the applied compression load, d_s is the distance between the two pairs of strain gauges, and Δ is the mid-height lateral deflection recorded by the LVDT. Note that Eq. (2) was derived by assuming that the structural behaviour was close to linear elastic, and it was thus suggested that no more than 15% of the expected failure load be used in the determination of e_m [25]. The overall loading eccentricities are positive if the knife-edges are located closer to the webs – see Fig. 8(a), but negative if the knife-edges are located near the flange tips – see Fig. 8(b). If the absolute value of the overall loading eccentricity $|e_m|$ exceeded $L_e/1000$, the position of the column specimen was carefully re-adjusted until the attainment of $|e_m|<L_e/1000$ [27–29]. Table 3 reports the final overall loading eccentricity of each channel section column specimen, with the largest normalised eccentricity $|e_m|/L_e$ equal to 1/1009.

$$e_m = \frac{EI(\varepsilon_{\max} - \varepsilon_{\min})}{Nd_s} - \Delta \quad (2)$$

All the examined press-braked S960 UHSS channel section column specimens underwent noticeable global deformations upon testing, and failed by member flexural buckling about the minor principal axes. It is worth noting that there were two orientations associated with minor-axis flexural buckling, namely 'C' orientation (indicating that specimens buckled towards the webs) and 'reverse C' orientation (indicating that specimens buckled towards the flange tips). With regard to channel section column specimens with negative overall loading eccentricities, the induced second-order bending moments resulted in compressive stresses at the flange tips; for these cases, the failure modes displayed minor-axis flexural buckling in the 'C' orientation, with a typical deformed failure specimen C1-L1 displayed in Fig. 9. Regarding channel section column specimens with positive overall loading eccentricities, the induced second-order bending moments led to tensile stresses at the flange tips, and the corresponding failure modes showed minor-axis flexural buckling in the 'reverse C' orientation, with a typical deformed failure specimen C2-L3 is presented in Fig. 10. The load–mid-height lateral deflection curves for the C 70×40×6 and C 80×45×6 column specimens are representatively shown in Figs 11(a) and 11(b), while the failure load $N_{u,test}$ and the corresponding mid-height lateral deflection at the failure load δ_u for each tested specimen are listed in Table 3; note that the mid-height lateral deflections are taken as negative for specimens failing by minor-axis flexural buckling in the 'C' orientation, but positive if the failure specimens buckle in the 'reverse C' orientation. It is worth noting that the behaviour and capacity of S960 UHSS channel section columns are different to their mild steel and S690 HSS counterparts. Specifically, the load–mid-height lateral deflection curves for S960 UHSS channel section columns were found to be shorter, indicating less ductile structural responses; this can be attributed to the distinct brittle nature of S960 ultra-high strength steel over mild steels and S690 high strength steel. The failure loads of S960 UHSS channel section columns were shown to be considerably larger than their mild steel and S690 HSS counterparts (particularly for those members with relatively short and intermediate lengths), owing to the much higher material strength. Moreover, the normalised failure loads of S960 UHSS channel section columns (by the cross-section yield loads) were found to be higher than those of mild steel and S690 HSS channel section columns, which can be attributed to the reduced sensitivity of S960 UHSS members to initial geometric imperfections [29]. Therefore, the codified design buckling curves, established for mild steel and S690 HSS channel section columns, were expected to be also applicable to the examined S960 UHSS channel section columns, as demonstrated in Section 4.

3. Numerical modelling

3.1. Overview

A numerical modelling programme was performed by means of the nonlinear finite element (FE) software ABAQUS [30], aimed at generating additional numerical results to supplement the test data, and reported in this section. The numerical modelling programme included a validation study to validate the developed column FE models against the experimental results and a parametric study to generate further numerical data over a broader spectrum of member lengths and cross-section sizes.

3.2. Development of FE models

Each channel section column FE model was developed using the S4R shell element [10,11,22,23] and based on the measured cross-section sizes and effective member length. Regarding the element width along the centreline of the cross-section, a uniform element width equal to the wall thickness t was assigned to the flat parts, while each corner of the cross-section was uniformly discretised into 6 elements to ensure an accurate representation of the curved geometry. The element length along the longitudinal direction of the channel section column FE model was equal to the wall thickness t. The measured engineering stress–strain curves from the tensile coupons C 70×40×6-W, C 70×40×6-F and C 70×40×6-C were converted into the true stress–true plastic strain curves, and then respectively assigned to the web, flanges and corners of each channel section column FE model. For ease of application of boundary conditions, each end section of the column FE model was coupled to a reference point positioned at the cross-section centroid. The reference point at one end was fully restrained except for rotation about the considered axis of buckling (i.e. the minor principle axis), whilst the reference point at the other end was allowed for translation in the longitudinal direction and rotation about the same axis, to replicate the pin-ended boundary condition that offered by the knife-edge and anchor devices in the tests. Initial global and local geometric imperfections were respectively incorporated into each channel section column FE model in the form of the lowest elastic global and local buckling mode shapes. Note that the global buckling mode shape of each column FE model was oriented such that it was consistent with the buckling orientation of the corresponding test specimen. The derived initial global geometric imperfection shape was factored by three different magnitudes – the measured overall loading eccentricity $|e_m|$ and two fractions of the member effective length (L_e/1000 and L_e/1500), while the obtained initial local geometric imperfection shape was scaled by three different values – the measured local geometric imperfection value ω_0 and two fractions of the wall thickness (t/100 and t/10). A total of five combinations of initial global and local geometric imperfection magnitudes were examined, aimed at evaluating the sensitivity of the developed channel section column FE models to geometric imperfection magnitudes and seeking the most appropriate imperfection magnitude combination to be employed in the parametric study.

3.3. Validation study

The modified Riks method is commonly adopted for solving static numerical problems with geometrical and material nonlinearities [10,11,22,23,30–32], and also employed in the present study for nonlinear analyses of the developed channel section column FE models. The derived numerical failure loads, load–mid-height lateral deflection curves and failure modes were compared against the corresponding experimental results, allowing for the accuracy of the developed channel section column FE models to be assessed. Table 4 presents the ratios of the FE to experimental failure loads $N_{u,FE}/N_{u,test}$; the results indicated that (i) the experimental failure loads were generally well predicted for all the five examined initial global and local geometric imperfection magnitude combinations, (ii) compared to the initial global geometric imperfection magnitudes, the initial local geometric imperfection magnitudes were found to be less influential on the failure loads, which may be attributed to the fact that the studied columns of non-slender channel section profiles are not prone to local instability, and (iii) the most accurate and consistent predictions of the experimental failure loads were obtained when the measured initial global and local geometric imperfection values were adopted, while precise failure load predictions were also achieved when the initial global and local geometric imperfection magnitudes are respectively taken as $L_e/1000$ and $t/10$. Moreover, the channel section column FE models are capable of simulating the experimental load–deformation histories, as evident in Figs 12(a) and 12(b), where the test and numerical load–mid-height lateral deflection curves for the two series of press-braked S960 UHSS channel section column specimens are compared. It is worth noting that the experimental and numerical load–lateral deflection curves for the specimens C1-L2 and C2-L2 have some discrepancies in the knee regions, with the main reason being that the actual initial geometric imperfections of the specimens and the idealised initial geometric imperfections (with elastic buckling mode shapes) of the FE modes are different. But the discrepancies were considered to be small and insignificant, and do not affect the failure loads. Figs 9 and 10 present comparisons between the experimentally and numerically obtained failure modes for typical specimens C1-L1 and C2-L3 failing by minor-axis flexural buckling in the 'C' and 'reverse C' orientations, respectively, revealing good agreement. Overall, it may be concluded that the developed FE models are capable of accurately simulating the test responses of pin-ended press-braked S960 UHSS channel section columns, and therefore deemed to be validated.

3.4. Parametric study

Having been validated in Section 3.3, the developed column FE models were subsequently used to conduct parametric studies, aimed at expanding the experimental data pool over a wide variety of effective member lengths and cross-section dimensions. The key geometric parameters of channel section column FE models are summarised in Table 5, where the outer web widths B_w are selected to be equal to 180 mm and 90 mm, with the outer flange widths B_f

varied to obtain a spectrum of cross-section aspect ratios B_w/B_f from 1.0 to 3.0, the wall thicknesses t are carefully selected such that all the modelled channel sections fall in the category of non-slender sections prescribed in EN 1993-1-12 [16], AISI S100 [13] and AS/NZS 4600 [14], and the effective member lengths are varied from 450 mm to 5150 mm so as to achieve a wide range of member non-dimensional slendernesses. In the parametric studies, the employed modelling procedures and techniques were in accordance with those described in Section 3.2, but with the initial global and local geometric imperfection magnitudes respectively fixed at $L_e/1000$ and $t/10$. Note that for each modelled channel section column, two orientations of initial global geometric imperfections were considered, enabling flexural buckling in both the 'C' and 'reverse C' orientations to be examined. The two sets of numerical parametric study results allowed for evaluation of the influence of flexural buckling orientations on the load-carrying capacities of press-braked S960 UHSS channel section columns. Overall, a total of 184 numerical results were derived in the parametric study.

4. Evaluation of applicability of international design standards

4.1. General

The current international design standards for cold-formed steel structures, as employed in Europe (EN 1993-1-3 [12]), North America (AISI S100 [13]) and Australia/New Zealand (AS/NZS 4600 [14]), are only applicable to members with material grades up to S700 (or S690), and thus none of these existing design standards can be directly applied to S960 UHSS members. In this section, the applicability of the codified design rules for S700 (S690) HSS press-braked channel section columns susceptible to minor-axis flexural buckling was evaluated for their S960 UHSS counterparts. Graphical and quantitative evaluations were both carried out through comparing the experimental (and numerical) failure loads N_u against the corresponding unfactored design flexural buckling strengths $N_{u,pred}$ obtained from each design standard, with the results respectively presented in Figs 13–18 and Table 6.

4.2. EN 1993-1-3 (EC3)

The current European code EN 1993-1-3 [12] covers the design of cold-formed steel structures with material grades up to S700. With regard to cold-formed steel columns prone to global instability (e.g., torsional, flexural and flexural-torsional buckling), the design procedures and formulations outlined in EN 1993-1-3 [12] were generally established by analogy with those for hot-rolled and welded normal strength steel columns prescribed in EN 1993-1-1 [15]. The concept of buckling curves, as derived based on the Perry-Robertson buckling formula, was employed in the European codes. For press-braked channel section column failing by flexural buckling about the minor principle axis, the EC3 strength prediction N_{EC3} can be determined from Eq. (2),

$$N_{EC3} = \chi A f_{ya} \tag{2}$$

where f_{ya} is the weighted average yield stress (by area), taking due account of the enhanced yield stress at corners due to cold-working during the press-braking process, and χ is the reduction factor and determined from the EC3 design buckling curves, as given by Eq. (4),

$$\chi = \frac{1}{\phi + \sqrt{\phi^2 - \overline{\lambda}^2}} \leq 1 \tag{4}$$

where ϕ is a buckling coefficient and can be calculated from Eq. (5), in which α is the imperfection factor, reflecting the degree of influence of initial geometric imperfections and residual stresses on the column buckling strengths, and dependent on the adopted design buckling curve; with regard to press-braked channel section columns failing by flexural buckling about the minor principal axes, buckling curve 'c' is prescribed in EN 1993-1-3 [12] and the corresponding α is taken as 0.49.

$$\phi = 0.5[1+\alpha(\bar{\lambda}-0.2)+\bar{\lambda}^2] \tag{5}$$

The applicability of the EC3 design buckling curve 'c' for S700 HSS press-braked channel section columns failing by minor-axis flexural buckling to their S960 UHSS counterparts was evaluated, based on the test and numerical data. The graphical evaluation results for press-braked S960 UHSS channel section columns with flexural buckling in the 'C' orientation and 'reverse C' orientation are depicted in Fig. 13 and Fig. 14, respectively, where the normalised test and numerical failure loads (by the cross-section yield loads Af_{ya}) are plotted against the member non-dimensional slendernesses $\bar{\lambda}$, and compared with the EC3 design buckling curve 'c'. In general, the EC3 buckling curve 'c' lies well below the test and numerical data points for press-braked S960 UHSS channel section columns with relatively short and intermediate member lengths (i.e. within the low and intermediate member non-dimensional slenderness range), but matches closely with data points for S960 UHSS channel section columns with relatively long member lengths (i.e. within the large member non-dimensional slenderness range). It was also found that channel section columns failing by flexural buckling in the 'reverse C' orientation generally exhibit superior strengths relative to their counterparts with flexural buckling in the 'C' orientation, especially in the low slenderness range; this can be attributed to the fact that second-order bending moments associated with 'C'-orientation flexural buckling induce additional compressive stresses at the outstand flanges and thus the specimens are more prone to failure and have relatively smaller load-carrying capacities [33]. The second-order bending moments associated with 'reverse C'-orientation flexural buckling induce additional compressive stresses at the corner regions and the specimens are thus less prone to instability. On this basis, and coupled with the fact that the pronounced material strain hardening of the corner regions can now be exploited, the specimens failing by flexural buckling in the 'reverse C' orientation have higher load-carrying capacities, in particular those relatively short columns with member non-dimensional slendernesses less than around 0.6, of which the failure loads are even greater than the cross-section yield loads. Figs 15 and 16 present the ratios of the test and numerical failure loads to the EC3 predicted flexural buckling strengths plotted against the member non-dimensional slendernesses $\bar{\lambda}$ for press-braked S960 UHSS channel section columns failing by minor-axis flexural buckling in the 'C' orientation and 'reverse C' orientation, respectively, whilst the mean ratios of N_u/N_{EC3} are equal to 1.13 and 1.27 for channel section columns with flexural buckling in the 'C' and 'reverse 'C' orientations, respectively, with the coefficients of variation (COVs) of 0.04 and 0.09, as listed in Table 6. Overall, it may be concluded that EC3 design buckling curve 'c' for S700 HSS press-braked channel section columns failing by minor-axis flexural buckling is also applicable to their S960 UHSS counterparts, but leads to overly conservative strength predictions for those relatively short and intermediate columns with failure in the 'reverse C' orientation.

4.3. AISI S100 (AISI) and AS/NZS 4600 (AS/NZS)

The North American Specification AISI S100 [13] and Australian/New Zealand Standard AS/NZS 4600 [14] are applicable to cold-formed steel structures with material grades up to S690, and employ the same provision for the design of concentrically loaded columns prone to global instability. The compressive strength N_{AISI} (or $N_{AS/NZS}$), as specified in AISI S100 [13] (or AS/NZS 4600 [14]), can be expressed as the product of the cross-section area A and the design failure stress f_n – see Eq. (6). The design failure stress f_n is derived from the design buckling curve, expressed by Eq. (7), where $\lambda_c=(f_y/f_{cre})^{0.5}$, where f_{cre} is given as the minimum of the member elastic flexural-torsional, flexural and torsional buckling stresses. It is worth noting that all the examined press-braked S960 UHSS channel section columns fail by minor-axis flexural buckling. Therefore, f_{cre} is taken as the corresponding elastic flexural buckling stress herein, and λ_c becomes essentially the same as $\bar{\lambda}$ employed in EN 1993-1-3 [12].

$$N_{AISI} = Af_n \text{ or } N_{AS/NZS} = Af_n \tag{6}$$

$$f_n = \begin{cases} \left(0.658^{\lambda_c^2}\right) f_{ya} & \text{for } \lambda_c \leq 1.5 \\ \left(\dfrac{0.877}{\lambda_c^{\;2}}\right) f_{ya} & \text{for } \lambda_c > 1.5 \end{cases} \tag{7}$$

The design buckling curve of AISI S100 [13] and AS/NZS 4600 [14] is also plotted with the test and numerical data in Figs 13 and 14 to access its applicability to press-braked S960 UHSS channel section columns. The AISI and AS/NZS design buckling curve is located slightly above the data points for columns with member non-dimensional slendernesses less than around 1.5 and failure in the 'C' orientation, but lies below the test and numerical data points for columns with member non-dimensional slendernesses less than around 1.5 and failure in the 'reverse C' orientation, while all the other data points are followed closely by the design curve. The AISI and AS/NZS design flexural buckling strengths were also assessed through graphical and numerical comparisons against the obtained test (and numerical) failure loads. Fig. 17 and Fig. 18 respectively display the graphical evaluation results for columns failing by flexural buckling in the 'C' and 'reverse C' orientations, indicating that AISI S100 [13] and AS/NZS 4600 [14] provide overall precise and consistent flexural buckling strength predictions, but with many unsafe design strengths for those short and intermediate columns failing in the 'C' orientation. The mean test and numerical to AISI (or AS/NZS) predicted failure load ratios N_u/N_{AISI} (or $N_u/N_{AS/NZS}$) are equal to 1.00 and 1.11, respectively, with the

COVs of 0.04 and 0.06, for press-braked S960 UHSS channel section columns with minor-axis flexural buckling in the 'C' and 'reverse C' orientations, as reported in Table 6. In comparison with EN 1993-1-3 [12], AISI S100 [13] and AS/NZS 4600 [14] were found to result in more accurate and consistent predictions of strengths for press-braked S960 UHSS channel section columns failing by minor-axis flexural buckling in both the 'C' and 'reverse C' orientations.

5. Conclusions

A thorough testing and numerical modelling programme has been carried out to investigate the structural behaviour and strengths of pin-ended press-braked S960 UHSS channel section columns prone to flexural buckling about the minor principle axes. The testing programme included concentrically loaded pin-ended column tests on ten press-braked S960 UHSS channel section columns with two cross-section sizes and various member lengths as well as supplementary measurements of their initial geometric imperfections. The obtained test results were used in the parallel numerical modelling programme for validating the developed column FE models, which were subsequently adopted to perform parametric studies to derive a numerical data pool on press-braked S960 UHSS channel section columns over an extended range of member lengths and cross-section dimensions. Two failure orientations associated with minor-axis flexural buckling of press-braked S960 UHSS channel section columns, namely 'C' orientation (indicating that columns buckled towards the webs) and 'reverse C' orientation (indicating that columns buckled towards the flange tips), were observed and discussed. It was found that channel section columns failing by flexural buckling in the 'reverse C' orientation exhibited superior load-carrying capacities than their counterparts with failure in the 'C' orientation. The derived experimental and numerical data was adopted to assess the applicability of the relevant design rules for S700 (or S690) HSS press-braked channel section columns failing by minor-axis flexural buckling, as prescribed in EN 1993-1-3 [12], AISI S100 [13] and AS/NZS 4600 [14], to the design of their S960 UHSS counterparts. EN 1993-1-3 [12] was found to yield a high degree of conservatism and scatter when used to predict the flexural buckling strengths for press-braked S960 UHSS channel section columns, especially those members with relatively short and intermediate lengths failing in the 'reverse C' orientation. AISI S100 [13] and AS/NZS 4600 [14] were found to yield more accurate and consistent predictions of flexural buckling strengths for press-braked S960 UHSS channel section columns than EN 1993-1-3 [12], but with many over-predicted flexural buckling strengths for those with short and intermediate member lengths failing in the 'C' orientation.

Acknowledgements

The authors are grateful to Mr. Subasanran Chelladurai for his assistance in the experiments. The research work described in this paper was supported by an Endowment Fund from Regency Steel Asia (RSA).

References

[1] Li D, Huang Z, Uy B, Thai H T, Hou C. Slenderness limits for fabricated S960 ultra-high-strength steel and composite columns. Journal of Constructional Steel Research 2019;159:109–121.

[2] SSAB. The beauty of Strenx: Stronger and Lighter. https://www.ssab.com/products/brands/strenx/products/strenx-960?accordion=downloads

[3] Azhari F, Hossain Apon A.-A, Heidarpour A, Zhao XL, Hutchinson C. Mechanical response of ultra-high strength (Grade 1200) steel under extreme cooling conditions, Construction and Building Materials 2018;175, 790–803.

[4] Nassirnia, M., Heidarpour, A., Zhao, XL, Minkkinen J. Innovative hollow columns comprising corrugated plates and ultra high-strength steel tubes, Thin-Walled Structures, 2016;101,14-25.

[5] Shi G, Zhou W, Lin C. Experimental investigation on the local buckling behavior of 960 MPa high strength steel welded section stub columns. Advances in Structural Engineering 2015;18(3):423–37.

[6] Ma J-L, Chan T-M, Young B. Experimental investigation on stub-column behavior of cold-formed high-strength steel tubular sections. Journal of Structural Engineering (ASCE) 2015;142(5):04015174.

[7] Ma J-L, Chan T-M, Young B. Experimental investigation of cold-formed high strength steel tubular beams. Engineering Structures 2016;126:200–9.

[8] Shi G, Ban H, Bijlaard FSK. Tests and numerical study of ultra-high strength steel columns with end restraints. Journal of Constructional Steel Research 2012;70:236–47.

[9] Ban H, Shi G, Shi Y, Bradford MA. Experimental investigation of the overall buckling behaviour of 960MPa high strength steel columns. Journal of Constructional Steel Research 2013;88:256–66.

[10] Wang F, Zhao O, Young B. Testing and numerical modelling of S960 ultra-high strength steel angle and channel section stub columns. Engineering Structures 2020;204:109902.

[11] Wang F, Zhao O, Young B. Flexural behaviour and strengths of press-braked S960 ultra-high strength steel channel section beams. Engineering Structures 2019;200:109735.

[12] EN 1993-1-3. Eurocode 3: Design of steel structures –Part 1-3: General rules — Supplementary rules for cold-formed members and sheeting. Brussels (Belgium): CEN; 2006.

[13] AISI S100. North American specification for the design of cold-formed steel structural members. American Iron and Steel Institute; 2016.

[14] AS/NZS 4600. Cold-formed steel structures. Sydney: AS/NZS 4600:2018; 2018.

[15] EN 1993-1-1. Eurocode 3: Design of steel structures – Part 1–1: General rules and rules for buildings. Brussels (Belgium): CEN; 2005.

[16] EN 1993-1-12. Eurocode 3: Design of steel structures – Part 1–12: Additional rules for the extension of EN 1993 up to steel grades S 700. Brussels (Belgium): CEN; 2007.

[17] American Society for Testing and Materials (ASTM). Standard test methods for tension testing of metallic materials. E8/E8M-15a, West Conshohocken, PA., USA: ASTM International; 2015.

[18] Young B, Dinis PB, Camotim D. CFS lipped channel columns affected by L-D-G interaction. Part I: Experimental investigation. Computers & Structures 2018;207:219–32.

[19] Rinchen R, Rasmussen KJR. Experiments on Long-Span Cold-Formed Steel Single C-Section Portal Frames. Journal of Structural Engineering (ASCE) 2020;146(1):04019187.

[20] Ye J, Hajirasouliha I, Becque J. Experimental investigation of local-flexural interactive buckling of cold-formed steel channel columns. Thin-Walled Structures 2018;125:245–58.

[21] Schafer B, Peköz T. Computational modeling of cold-formed steel: characterizing geometric imperfections and residual stresses. Journal of constructional steel research 1998;47:193–210.

[22] Zhang L, Wang F, Liang Y, Zhao O. Press-braked S690 high strength steel equal-leg angle and plain channel section stub columns: Testing, numerical simulation and design. Engineering Structures 2019;201:109764.

[23] Liang Y, Zhao O, Long Y, Gardner L. Stainless steel channel sections under combined compression and minor axis bending–Part 1: Experimental study and numerical modelling. Journal of constructional steel research 2019;152:154–61.

[24] Chen M-T, Young B. Tests of cold-formed steel semi-oval hollow section members under eccentric axial load. Journal of Structural Engineering (ASCE) 2020;146(4):04020027.
[25] Zhao O, Gardner L, Young B. Experimental Study of Ferritic Stainless Steel Tubular Beam-Column Members Subjected to Unequal End Moments. Journal of Structural Engineering (ASCE) 2016;142(11):04016091.
[26] Chen M-T, Young B. Beam-column tests of cold-formed steel elliptical hollow sections. Engineering Structures 2020;207:109911.
[27] Rasmussen KJR, Hancock GJ. Tests of high strength steel columns. Journal of Constructional Steel Research 1995;34:27–52.
[28] Buchanan C, Real E, Gardner L. Testing, simulation and design of cold-formed stainless steel CHS columns. Thin-Walled Structures 2018;130:297–312.
[29] Wang J, Gardner L. Flexural Buckling of Hot-Finished High-Strength Steel SHS and RHS Columns. Journal of Structural Engineering (ASCE) 2017;143(6):04017028.
[30] ABAQUS. ABAQUS/standard user's manual. Version 6.17. Dassault Systemes Simulia Corp. USA; 2017.
[31] Roy K, Ting TCH, Lau HH, Lim JBP. Nonlinear behaviour of back-to-back gapped built-up cold-formed steel channel sections under compression. Journal of Constructional Steel Research 2018;147:257–76.
[32] Becque J, Rasmussen KJR. A numerical investigation of local–overall interaction buckling of stainless steel lipped channel columns. Journal of Constructional Steel Research 2009;65:1685–93.
[33] Rasmussen K, Hancock G. Design of thin-walled plain channel section columns against flexural buckling. Thin-Walled structures 1994;20:219–40.

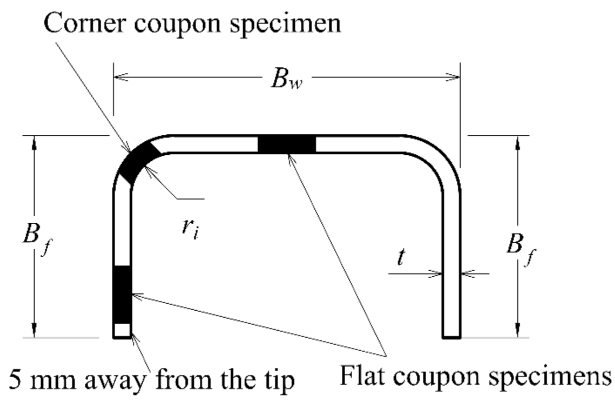

Fig. 1. Definition of symbols and locations of tensile coupons extracted from channel section.

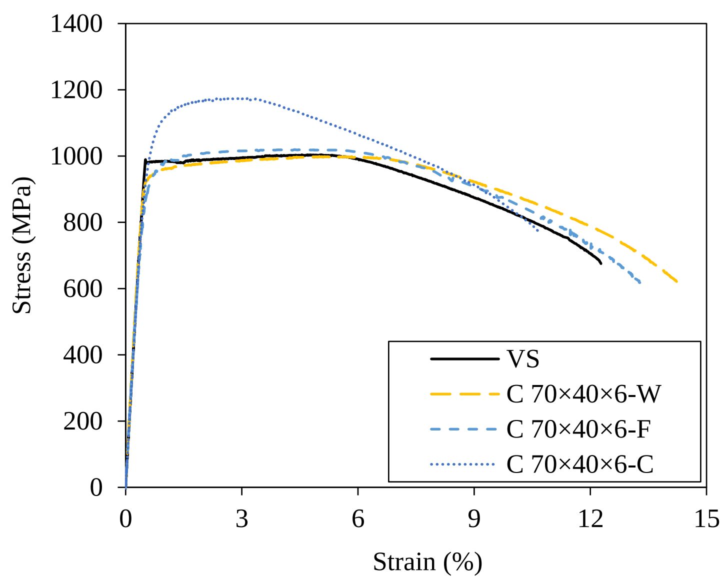

Fig. 2. Stress–strain curves obtained from tensile coupon tests [10].

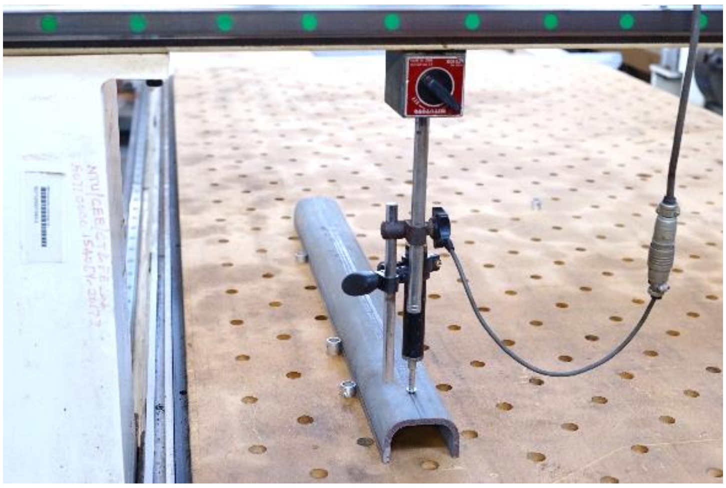

(a) Setup for initial global geometric imperfection measurements

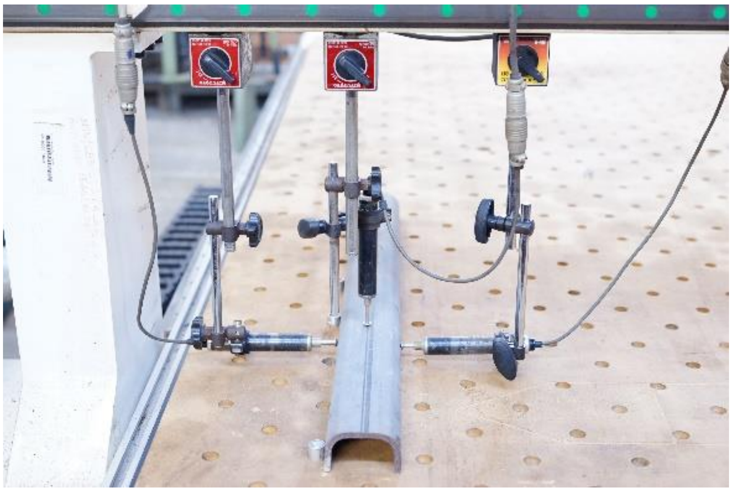

(b) Setup for initial local geometric imperfection measurements

Fig. 3. Setups for initial geometric imperfection measurements.

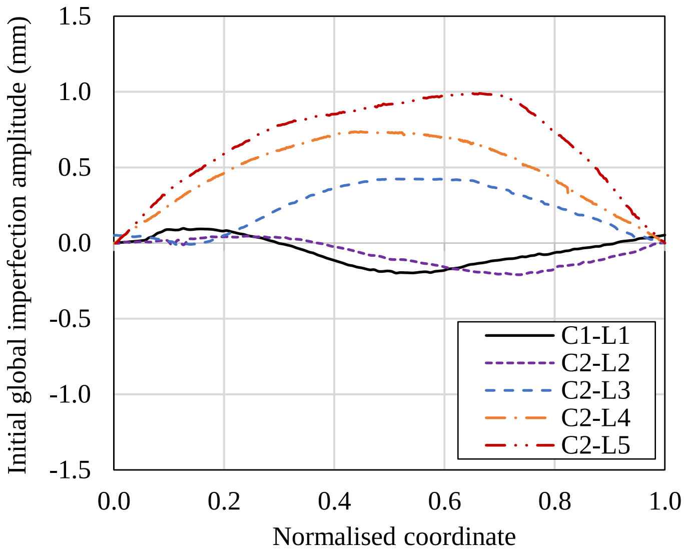

(a) C 70×40×6 column specimens

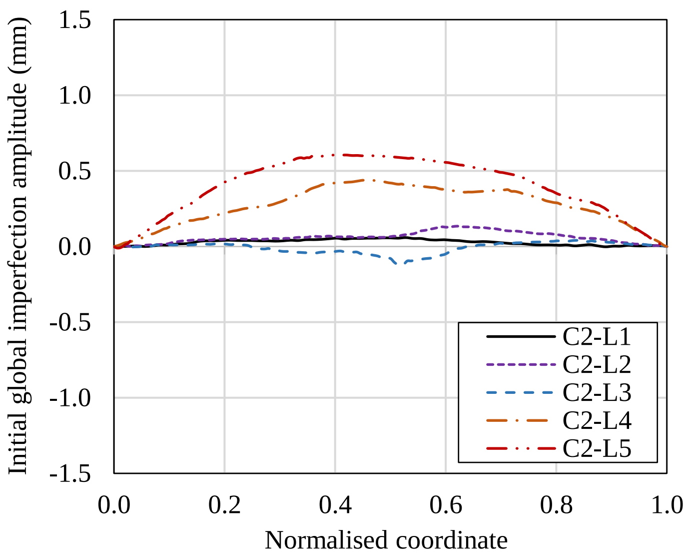

(b) C 80×45×6 column specimens

Fig. 4. Measured initial global geometric imperfection distributions of press-braked S960 UHSS channel section column specimens.

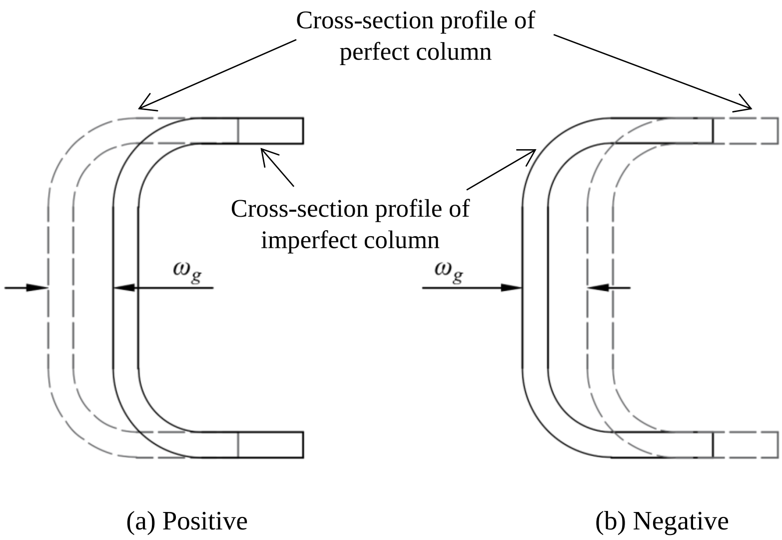

Fig. 5. Sign convention of initial global geometric imperfection amplitude ω_g.

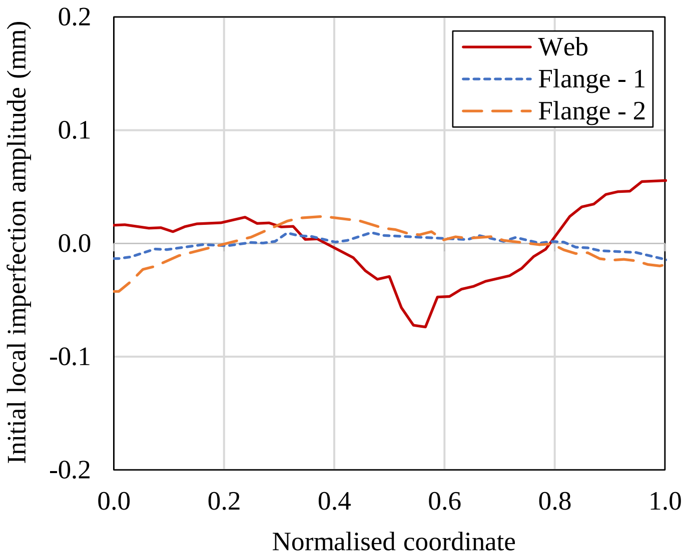

Fig. 6. Measured initial local geometric imperfection distributions for a typical column specimen C2-L3.

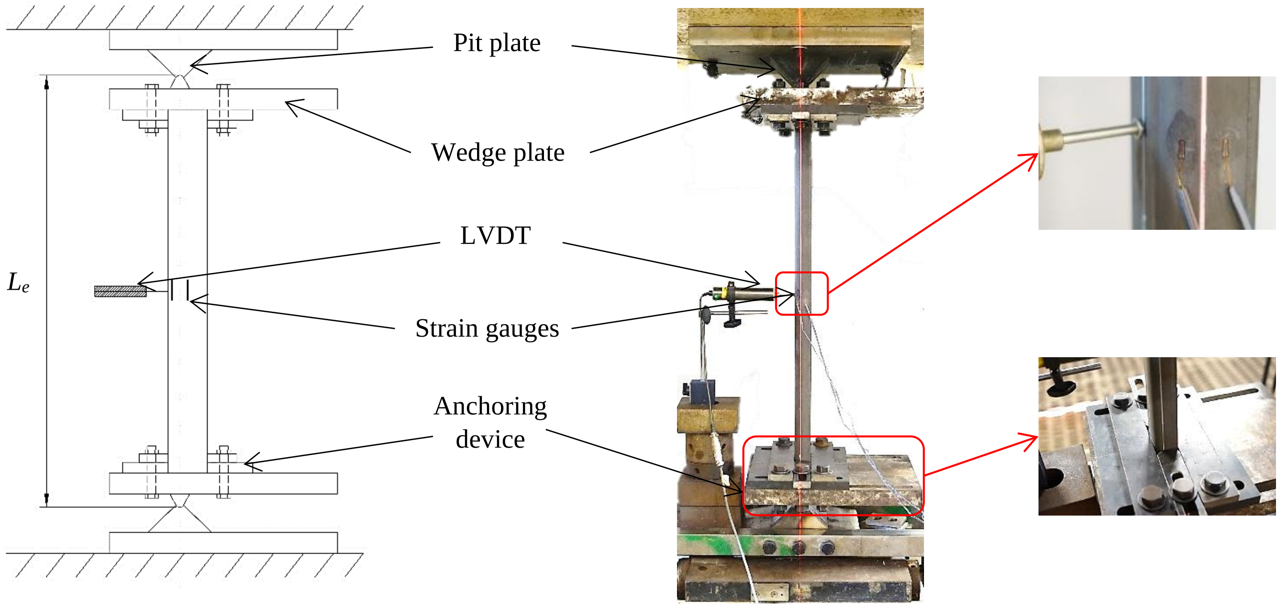

Fig. 7. Experimental setup for pin-ended press-braked S960 UHSS channel section columns.

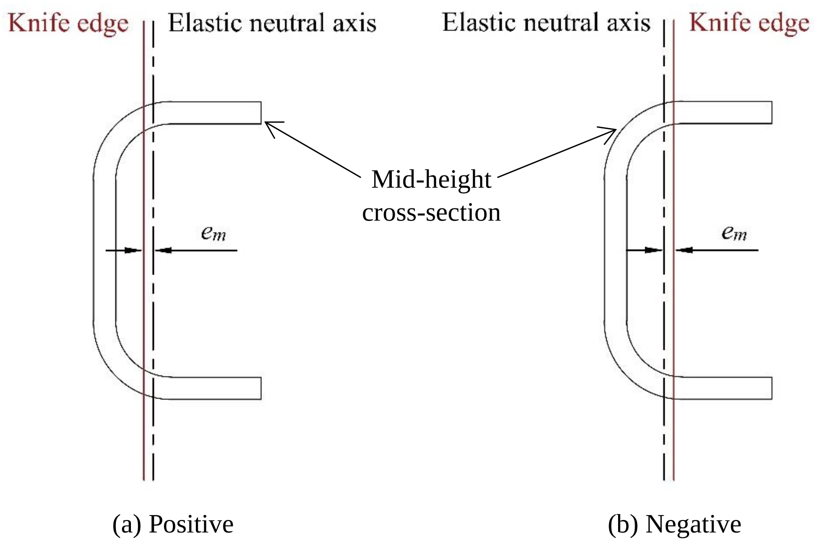

Fig. 8. Sign convention of overall loading eccentricity e_m.

Fig. 9. Experimental and numerical failure modes for press-braked S960 UHSS channel section column specimen C1-L1.

Fig. 10. Experimental and numerical failure modes for press-braked S960 UHSS channel section column specimen C2-L3.

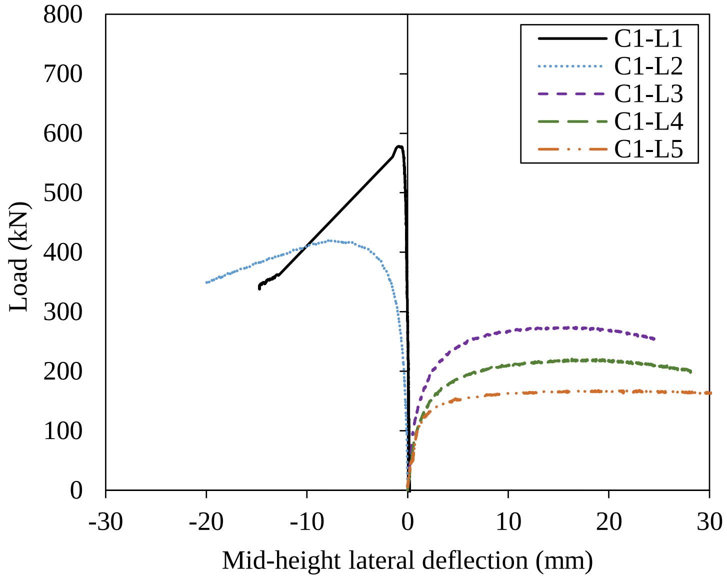

(a) C 70×40×6 column specimens

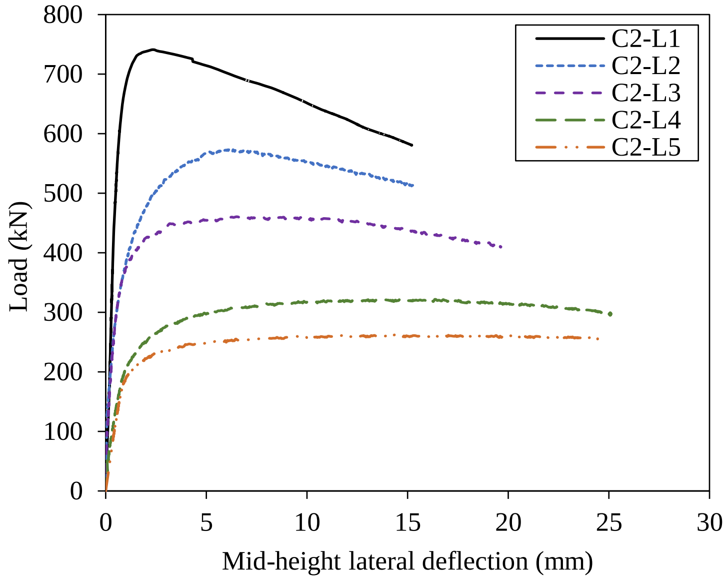

(b) C 80×45×6 column specimens

Fig. 11. Experimental load–mid-height lateral deflection curves for pin-ended press-braked S960 UHSS channel section column specimens.

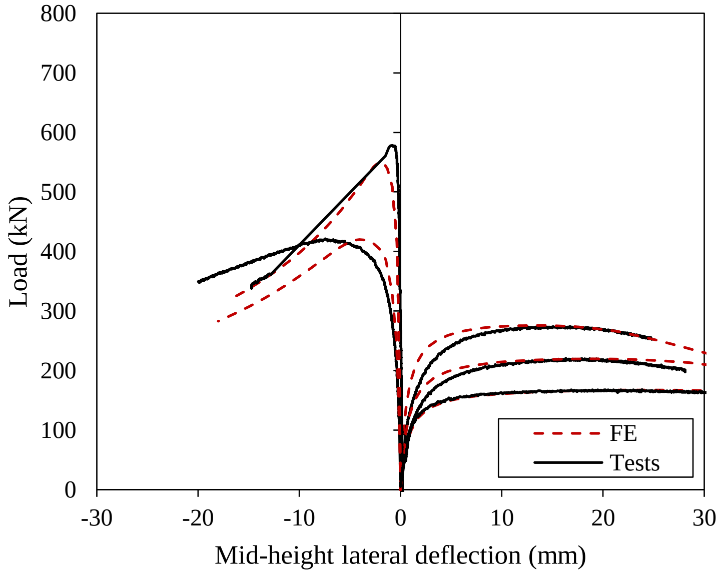

(a) C 70×40×6 column specimens

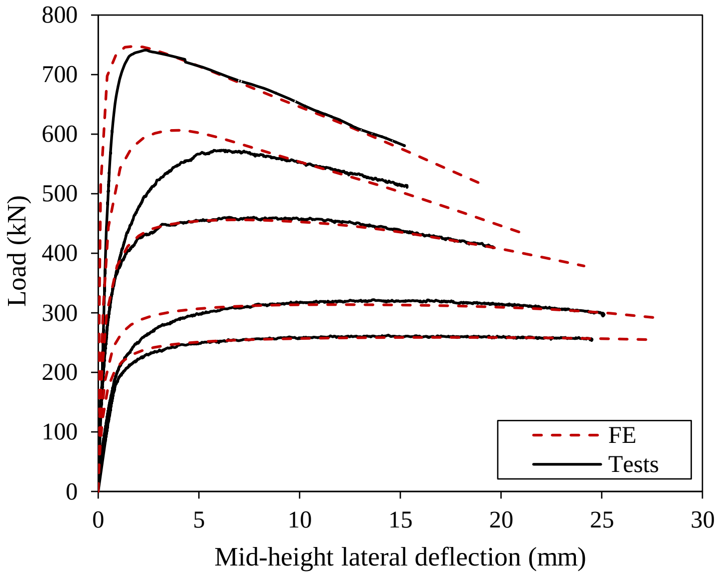

(b) C 80×45×6 column specimens

Fig. 12. Experimental and numerical load–mid-height lateral deflection curves for pin-ended press-braked S960 UHSS channel section column specimens.

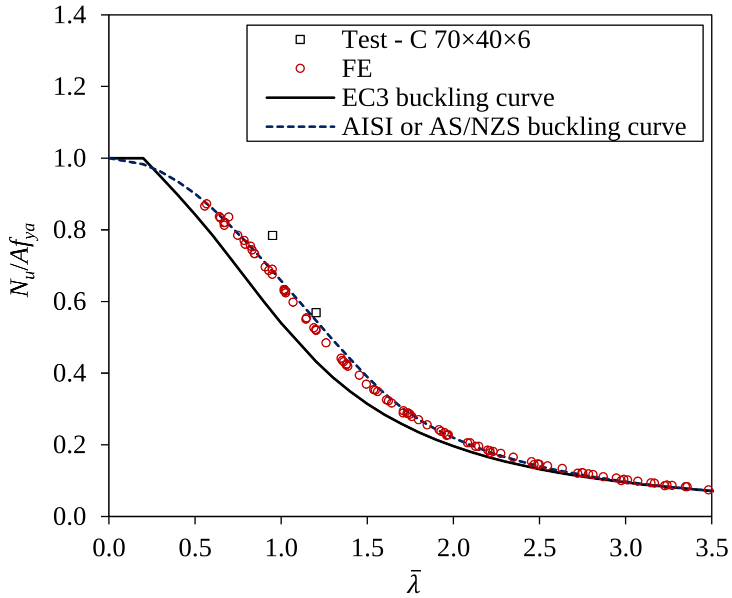

Fig. 13. Comparisons of test and FE failure loads with design buckling curves for press-braked S960 UHSS channel section columns with flexural buckling in the 'C' orientation.

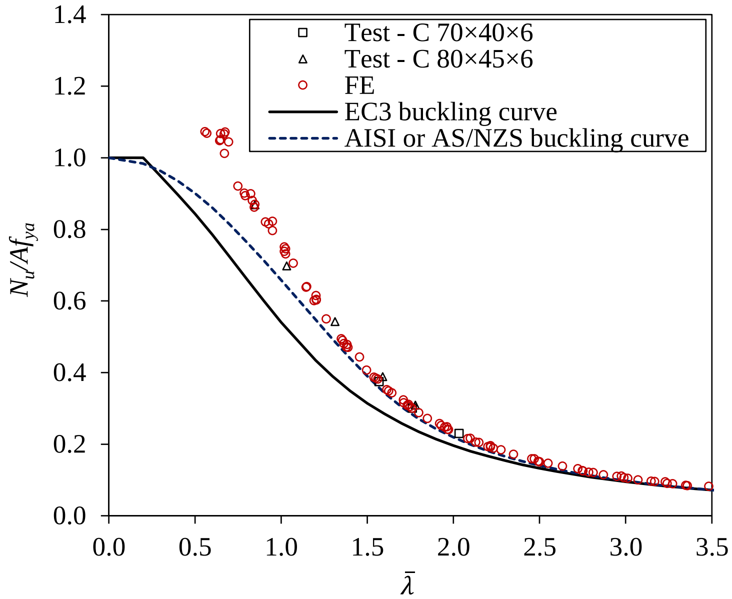

Fig. 14. Comparisons of test and FE failure loads with design buckling curves for press-braked S960 UHSS channel section columns with flexural buckling in the 'reverse C' orientation.

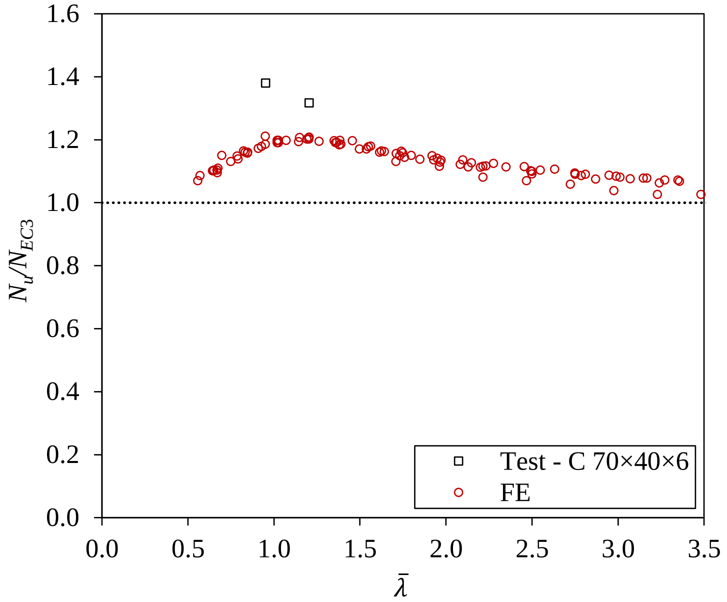

Fig. 15. Comparisons of test and FE failure loads with EC3 predicted strengths for press-braked S960 UHSS channel section columns with flexural buckling in the 'C' orientation.

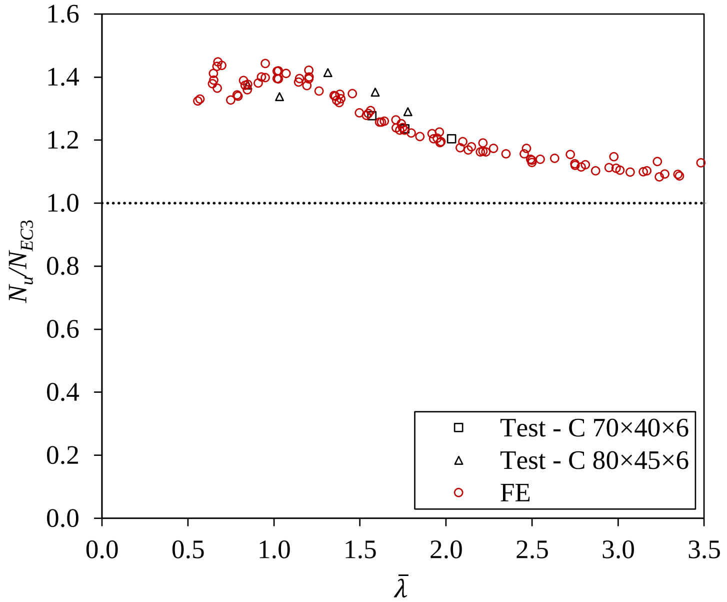

Fig. 16. Comparisons of test and FE failure loads with EC3 predicted strengths for press-braked S960 UHSS channel section columns with flexural buckling in the 'reverse C' orientation.

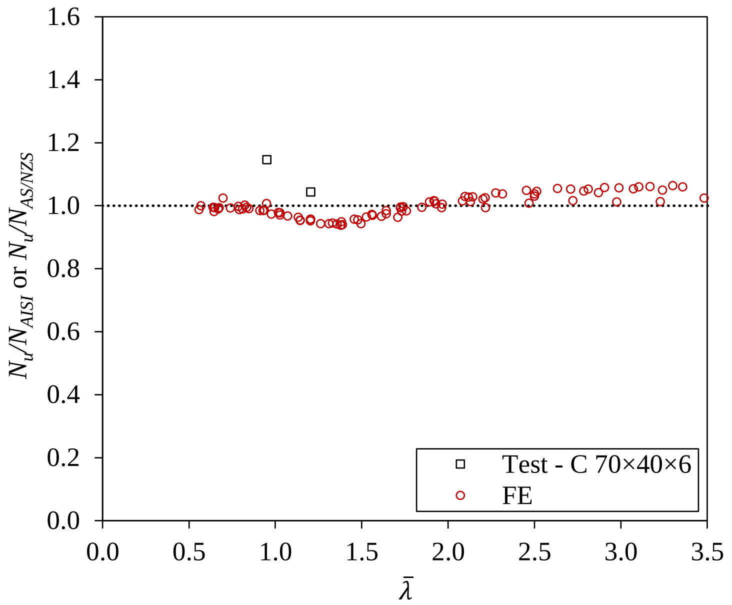

Fig. 17. Comparisons of test and FE failure loads with AISI (or AS/NZS) predicted strengths for press-braked S960 UHSS channel section columns with flexural buckling in the ‘C’ orientation.

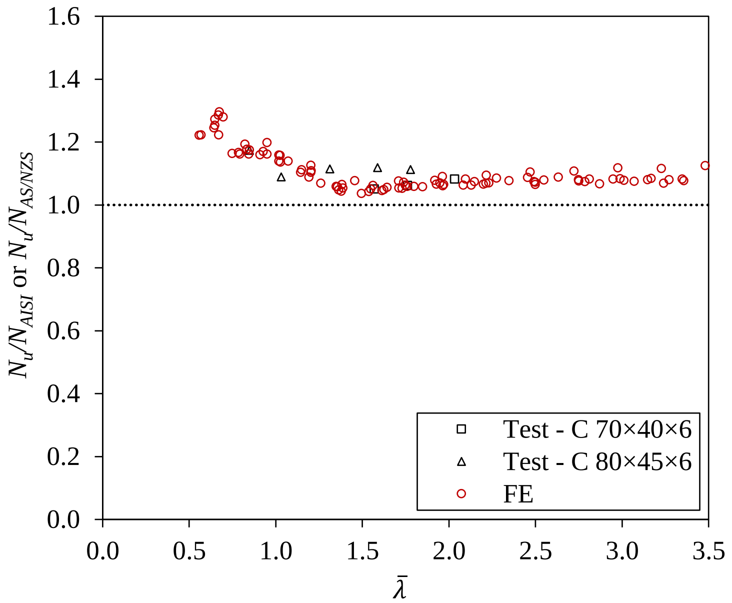

Fig. 18. Comparisons of test and FE failure loads with AISI (or AS/NZS) predicted strengths for press-braked S960 UHSS channel section columns with flexural buckling in the ‘reverse C’ orientation.

Table 1. Measured geometric dimensions and initial geometric imperfections of press-braked S960 UHSS channel section column specimens.

Cross-section	Specimen ID	L (mm)	B_f (mm)	B_w (mm)	t (mm)	r_i (mm)	ω_0 (mm)	ω_g (mm)
C 70×40×6	C1-L1	400.2	41.41	69.26	6.04	14.8	0.07	-0.26
	C1-L2	549.8	41.62	68.55	6.10	14.8	0.08	-0.21
	C1-L3	698.9	39.09	73.35	6.02	14.8	0.02	0.42
	C1-L4	849.0	40.72	70.86	6.01	14.8	0.08	0.74
	C1-L5	1000.0	40.64	69.41	6.07	14.8	0.01	0.99
C 80×45×6	C2-L1	400.1	45.94	79.25	6.10	14.5	0.02	0.06
	C2-L2	499.9	44.69	78.25	6.01	14.5	0.03	0.14
	C2-L3	698.5	45.78	79.67	6.07	14.5	0.07	-0.12
	C2-L4	849.0	44.66	78.18	6.08	14.5	0.04	0.44
	C2-L5	999.0	45.78	79.56	6.09	14.5	0.02	0.61

Table 2. Measured flat and corner material properties of press-braked S960 UHSS channel section C 70×40×6 and virgin sheet [10].

Coupon specimen ID	E (GPa)	f_y (MPa)	f_u (MPa)	ε_u (%)	ε_f (%)	f_u/f_y
VS	208	982	1011	5.1	12.3	1.03
C 70×40×6-W	214	935	1000	4.5	14.3	1.07
C 70×40×6-F	203	927	1021	5.1	13.3	1.10
C 70×40×6-C	203	1033	1173	2.4	10.6	1.13

Table 3. Test results for press-braked S960 UHSS channel section column specimens.

Cross-section	Specimen ID	L_e (mm)	e_m (mm)	$\|e_m\|/L_e$	$N_{u,test}$ (kN)	δ_u (mm)	Failure orientation
C 70×40×6	C1-L1	550.2	-0.10	1/5342	578.3	-0.8	C
	C1-L2	699.8	-0.16	1/4401	421.5	-7.4	C
	C1-L3	848.9	0.82	1/1030	274.0	15.0	reverse C
	C1-L4	999.0	0.99	1/1009	220.8	16.3	reverse C
	C1-L5	1150.0	1.02	1/1127	168.2	23.9	reverse C
C 80×45×6	C2-L1	550.1	0.46	1/1198	741.1	2.8	reverse C
	C2-L2	649.9	0.64	1/1023	573.3	6.2	reverse C
	C2-L3	848.5	0.52	1/1622	460.6	7.7	reverse C
	C2-L4	999.0	0.50	1/2002	322.2	13.7	reverse C
	C2-L5	1149.0	0.50	1/2293	262.7	14.4	reverse C

Table 4. Comparison of press-braked S960 UHSS channel section column FE and test failure loads for various initial geometric imperfection magnitude combinations.

Cross-section	Specimen ID	$N_{u,FE}/N_{u,test}$				
		$\omega_0+\|e_m\|$	$t/100+L_e/1000$	$t/100+L_e/1500$	$t/10+L_e/1000$	$t/10+L_e/1500$
C 70×40×6	C1-L1	0.95	0.88	0.91	0.88	0.90
	C1-L2	1.00	0.92	0.95	0.92	0.95
	C1-L3	1.01	1.00	1.03	1.00	1.03
	C1-L4	1.00	1.01	1.01	0.99	1.01
	C1-L5	1.00	0.98	1.00	0.98	1.00
C 80×45×6	C2-L1	1.01	1.00	1.02	1.00	1.03
	C2-L2	1.06	1.06	1.09	1.06	1.10
	C2-L3	0.99	0.96	0.99	0.96	0.99
	C2-L4	0.97	0.97	0.99	0.97	0.99
	C2-L5	0.98	0.98	0.99	0.98	0.99
Mean		1.00	0.98	1.00	0.97	1.00
COV		0.03	0.05	0.05	0.05	0.05

Table 5. Geometric dimensions of press-braked S960 UHSS channel section columns selected for parametric studies.

B_w (mm)	B_f (mm)	t (mm)	Cross-section class*	Aspect ratio B_w/B_f	L_e (mm)
180	60	10	1	3.00	450, 550, 650, 750, 950, 1150, 1350, 1550, 1750, 1950, 2150, 2350, 2550, 2750
180	120	15	2	2.25	950, 1150, 1350, 1550, 1750, 1950, 2150, 2350, 2550, 2750, 2950, 3150, 3350, 3550, 3750
180	160	16	3	1.13	1550, 1950, 2350, 2750, 3150, 3550, 3750, 3950, 4150, 4550, 5150
90	50	7	1	1.80	450, 550, 650, 750, 950, 1150, 1350, 1550, 1750, 1950, 2150, 2350, 2550, 2750, 2950
90	80	10	2	1.13	750, 950, 1150, 1350, 1550, 1750, 1950, 2150, 2350, 2550, 2750, 2950, 3150, 3350, 3550
90	70	8	3	1.29	650, 750, 950, 1150, 1350, 1550, 1750, 1950, 2150, 2350, 2550, 2750, 2950, 3150, 3350
90	40	7	1	2.25	350, 450, 550, 650, 750, 950, 1150, 1350, 1550, 1750

Note: * The cross-section class is defined according to EN 1993-1-1 [15] and EN 1993-1-12 [16].

Table 6. Comparisons of test and FE failure loads with predicted flexural buckling strengths.

Failure orientation	No. of data		N_u/N_{EC3}		N_u/N_{AISI}		$N_u/N_{AS/NZS}$	
	Test	FE	Mean	COV	Mean	COV	Mean	COV
C	2	92	1.13	0.04	1.00	0.04	1.00	0.04
reverse C	8	92	1.27	0.09	1.11	0.06	1.11	0.06
Total	10	184	1.21	0.09	1.06	0.07	1.06	0.07